Thin Solid Films 518 (2010) 7174–7182

Contents lists available at ScienceDirect

Thin Solid Films

journal homepage: www.elsevier.com/locate/tsf

Effect of vacuum magnetic annealing on the structural and physical properties of the Ni and Al co-doped ZnO films

Mingpeng Yu [a], Hong Qiu [a,*], Xiaobai Chen [b]

[a] Department of Physics, School of Applied Science, University of Science and Technology Beijing, 30 Xueyuan Road, Haidian District, Beijing 100083, China
[b] College of Mechanical Engineering, Beijing Technology and Business University, Beijing 100048, China

ARTICLE INFO

Article history:
Received 14 October 2009
Received in revised form 9 July 2010
Accepted 12 July 2010
Available online 16 July 2010

Keywords:
Ni and Al co-doped Zinc oxide
Thin films
Magnetic annealing
Structural properties
Ferromagnetism
Carrier transport
Magnetization behavior
Sputtering

ABSTRACT

About 300 nm-thick $Zn_{0.87}Al_{0.06}Ni_{0.07}O$, $Zn_{0.83}Al_{0.06}Ni_{0.11}O$ and $Zn_{0.81}Al_{0.04}Ni_{0.15}O$ films were deposited on glass substrates at 300 K by co-sputtering ZnO:Al and Ni targets. The films were annealed in vacuum at 673 K for 2 h under a magnetic field of 4.8×10^4 A/m applied along the film plane and then were cooled down to room temperature without magnetic field. All the films have a wurtzite structure and consist of thin columnar grains perpendicular to the substrate. The annealing promotes the (002) orientation growth in the film growing direction for the $Zn_{0.87}Al_{0.06}Ni_{0.07}O$ and $Zn_{0.83}Al_{0.06}Ni_{0.11}O$ films as well as the (100) orientation growth for the $Zn_{0.81}Al_{0.04}Ni_{0.15}O$ film. The annealing results in a slight increase in the grain size. A weak Ni diffraction peak was detected for the annealed films with high Ni content. The annealing enhances the room temperature ferromagnetism of the films. A temperature dependence of magnetization confirms that the Curie temperature is above 400 K for the annealed films. The films magnetically annealed exhibit an anisotropic magnetization behavior. The annealed $Zn_{0.87}Al_{0.06}Ni_{0.07}O$ film has the lowest resistivity ($8.73\times10^{-3}\,\Omega$ cm), the highest free electron concentration (1.73×10^{20} cm^{-3}) and Hall mobility (4.16 cm^{2}V^{-1} s^{-1}). A temperature dependence of the resistivity from 50 K to 300 K reveals that the carrier transport mechanism is Mott's variable range hopping in the low temperature range and thermally activated band conduction in the high temperature range.

1. Introduction

ZnO films co-doped with Al and transition metals are important function materials for optoelectronic and magnetoelectronic applications. The transition metals generally used are Co and Mn [1–5]. Recently, we have prepared the Ni and Al co-doped ZnO films on glass substrates by direct current (DC) magnetron co-sputtering [6,7]. The films had the room temperature ferromagnetism, dependent on the deposition temperature and the Ni content. Furthermore, the film, which exhibited the better ferromagnetic behavior, had the relatively high resistivity. It is a significant work to prepare the Ni and Al co-doped ZnO films having better electrical and ferromagnetic behaviors for their potential applications.

Annealing could improve the structural and physical properties of ZnO films doped with transition metals. Cho et al. [8] heat-treated CoFe doped ZnO films at 823 K for 10 min by rapid thermal annealing under vacuum. They found that the rapid thermal annealing led to a remarked increase in the magnetization and the electron concentration of the films. Hsu et al. [9] investigated systematically the annealing effect on structure and magnetism for Co doped ZnO films under air, Ar and Ar/H_2 atmospheres at 523 K. The saturation magnetization varied drastically for the different annealing processes. They found that the ferromagnetism of the films was strongly correlated with the oxygen vacancies in the ZnO lattice. Khare et al. [10] annealed $Zn_{0.98}Co_{0.02}O$ films in reducing or oxidizing atmosphere at 673 K. They observed that the magnetization of the film decreased after every annealing regardless of reducing or oxidizing atmosphere. Huang et al. [11] reported that for the Co doped ZnO films annealed in air the saturation magnetization decreased with increasing annealing temperature. Liu et al. [12] sputter-deposited Ni doped ZnO films and heat-treated them by rapid thermal annealing at 1073 K for 10 min in Ar gas environment. They found that the heat-treatment increased markedly the magnetization of the films and destroyed the ZnO crystallinity.

Among many techniques to prepare materials, magnetic field annealing plays an important role on microstructures and magnetic properties of the magnetic materials. Harada et al. [13] reported an effect of magnetic field annealing on grain growth in nanocrystalline Ni produced by electrodeposition. Chung et al. [14] found that Ni tapes magnetically annealed showed a stronger texture and a better magnetic domain structure than those annealed without magnetic field. Coisson et al. [15] prepared 30 nm-thick $Co_{50}Fe_{50}$ films on glass substrates by sputtering and annealed the films under a magnetic field of 100 Oe. They found that the magnetic field annealing affected the

* Corresponding author. Tel.: +86 10 62333786.
E-mail address: qiuhong@sas.ustb.edu.cn (H. Qiu).

0040-6090/$ – see front matter © 2010 Elsevier B.V. All rights reserved.
doi:10.1016/j.tsf.2010.07.045

ferromagnetic behaviors of the films. It has not been reported how a vacuum magnetic annealing influences structural and physical properties of the ZnO-based films doped with transition metals. In the present work, $Zn_{0.87}Al_{0.06}Ni_{0.07}O$, $Zn_{0.83}Al_{0.06}Ni_{0.11}O$ and $Zn_{0.81}Al_{0.04}Ni_{0.15}O$ films are deposited on glass substrates at 300 K by co-sputtering ZnO:Al and Ni targets. Then the films are annealed in vacuum under a magnetic field applied along the film plane. The structure of the films is studied using X-ray diffraction (XRD), atomic force microscopy (AFM) and field emission scanning electron microscopy (FE-SEM). The magnetic, electrical and semiconducting properties are measured by using a vibrating sample magnetometer (VSM) and the van der Pauw method. A carrier transport mechanism is discussed by measuring the temperature-dependent resistivity of the films.

2. Experimental procedure

The DC magnetron sputtering system used (KYKY Technology Development Ltd.), which has two targets inclined at an angle of 45° to the same substrate, has been described elsewhere in detail [16]. One target was a sintered ceramic ZnO + 2 wt.%Al_2O_3 target (99.99% in purity) with 50 mm in diameter and the other was a Ni target (99.99% in purity) with 50 mm in diameter. The distance between the target and the substrate was about 100 mm. A load-lock chamber was used to prevent the working chamber from air during changing a sample. The glass substrates were ultrasonically rinsed in acetone, in deionized water and in ethanol. About 300 nm-thick Ni and Al co-doped ZnO films were deposited on glass substrates at 300 K by co-sputtering under an Ar gas (99.9995% in purity) pressure of 1 Pa. During the sputter-deposition, the sputtering power applied to the ZnO + 2 wt.%Al_2O_3 target was fixed at 200 W and that applied to the Ni target was respectively adjusted to 10 W, 14 W and 18 W in order to control the Ni content in the films. According to the energy dispersive X-ray spectroscopy analysis, the $Zn_{0.87}Al_{0.06}Ni_{0.07}O$, $Zn_{0.83}Al_{0.06}Ni_{0.11}O$ and $Zn_{0.81}Al_{0.04}Ni_{0.15}O$ films were obtained. The deposition rate was about 0.25 nm/s and the deposition time was 20 min. The substrate holder was rotated using a stepping motor during deposition in order to obtain a uniformly thick film. Prior to deposition, the working chamber was evacuated to a pressure lower than 2×10^{-4} Pa using a turbo molecular pump.

Magnetic annealing was carried out in vacuum lower than 2×10^{-3} Pa. After the heat-treatment chamber was evacuated using a turbo molecular pump, the Ni and Al co-doped ZnO films were heated to 673 K without magnetic field and then were annealed at 673 K for 2 h under a magnetic field of 4.8×10^4 A/m applied along the film plane. Finally, the films were cooled down to room temperature without magnetic field.

XRD (Rigaku Co.) was used to analyze the crystalline orientation and the lattice constant of the films. The XRD measurements were performed in a standard θ–2θ scan using a Cu Kα radiation filtered by a crystal monochromator (wavelength λ = 0.15417 nm). The X-ray source was operated at a power of 40 kV × 200 mA. Scan speed was 0.1 deg/s and scan step was 0.02° . FE-SEM (Zeiss Co.) was used to observe the crystalline structure of the films. Surface smoothness and morphology of the films were investigated using AFM of CSPM5000 (Ben Yuan Ltd.).

A magnetization curve of the films was measured at room temperature using VSM (Quantum Design Co.). The magnetic field was applied along the film plane during the VSM measurement. The magnetization data of the film were calibrated by subtracting the signal of the substrate. A temperature dependence of the magnetization for the annealed Ni and Al co-doped films was measured from 50 K to 400 K. First, the film was cooled down to 50 K at zero field. Then the magnetization data were taken with warming up under a magnetic field of 8.0×10^4 A/m applied along the film plane. The warming rate is approximate to 5 K/min. The resistivity and the Hall coefficient of the films were measured at room temperature using the van der Pauw method. The carrier concentration and the Hall mobility were calculated in terms of the resistivity and the Hall coefficient. A temperature dependence of the resistivity for the films was measured in the temperature range of 50–300 K (Quantum Design Co.).

3. Results and discussion

3.1. Structure

Fig. 1 shows XRD patterns of the Ni and Al co-doped ZnO films as-deposited and magnetically annealed. As can be seen from Fig. 1, all the films have a wurtzite structure. For the as-deposited films, the ZnO(100), ZnO(002), ZnO(101) and ZnO(110) diffraction peaks are observed. For the annealed films, the $Zn_{0.87}Al_{0.06}Ni_{0.07}O$ and $Zn_{0.83}Al_{0.06}Ni_{0.11}O$ films mainly show the ZnO(002) peak and the $Zn_{0.81}Al_{0.04}Ni_{0.15}O$ film mainly exhibits the ZnO(100) peak. It indicates that the annealing promotes c-axis preferential orientation growth for the $Zn_{0.87}Al_{0.06}Ni_{0.07}O$ and $Zn_{0.83}Al_{0.06}Ni_{0.11}O$ films as well as the (100) preferential orientation growth for the $Zn_{0.81}Al_{0.04}Ni_{0.15}O$ film. Using the measured XRD peak intensity, the texture coefficient Y(hkl) of a plane (hkl) for the film can be given by

$$Y(hkl) = \frac{I(hkl)/I_b(hkl)}{\sum(1/N)\times[I(hkl)/I_b(hkl)]} \quad (1)$$

where I(hkl) is the measured XRD peak intensity of the plane (hkl) of the film, I_b(hkl) the standard XRD peak intensity of the plane (hkl) and N the number of the reflection diffraction peak [17]. In this case, the value of I_b(hkl) comes from that of the ZnO bulk [18]. The Y values of the as-deposited films are summarized in Table 1. As shown in Table 1, for the as-deposited films the c-axis preferential orientation in the film growing direction weakens with increasing the Ni content. It is consistent with the result reported previously [7]. It is considered that large amounts of Ni atoms as impurity influence a nucleation at

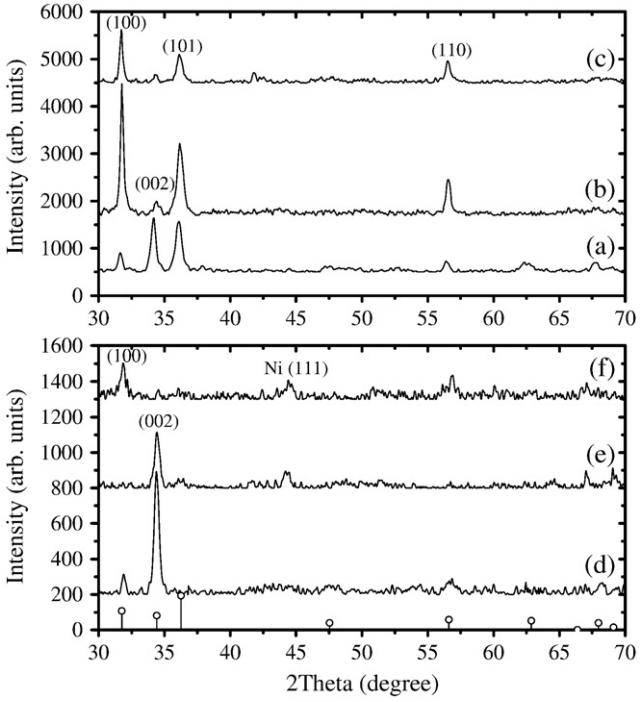

Fig. 1. XRD patterns of the Ni and Al co-doped ZnO films; (a) $Zn_{0.87}Al_{0.06}Ni_{0.07}O$ film, as-deposited, (b) $Zn_{0.83}Al_{0.06}Ni_{0.11}O$ film, as-deposited, (c) $Zn_{0.81}Al_{0.04}Ni_{0.15}O$ film, as-deposited, (d) $Zn_{0.87}Al_{0.06}Ni_{0.07}O$ film, annealed, (e) $Zn_{0.83}Al_{0.06}Ni_{0.11}O$ film, annealed, (f) $Zn_{0.81}Al_{0.04}Ni_{0.15}O$ film, annealed. The standard diffraction pattern of wurtzite hexagonal ZnO is also shown.

Table 1
Texture coefficients Y of the as-deposited films.

Film	$Y(100)$	$Y(002)$	$Y(101)$	$Y(110)$
$Zn_{0.87}Al_{0.06}Ni_{0.07}O$	0.75	1.97	0.81	0.47
$Zn_{0.83}Al_{0.06}Ni_{0.11}O$	1.66	0.60	0.72	1.02
$Zn_{0.81}Al_{0.04}Ni_{0.15}O$	1.57	0.58	0.60	1.25

the initial stage of the film growth and incorporate in the growing films, resulting in a deterioration of the c-axis preferential orientation of the films. No diffraction peaks of Ni, Al and their oxides are detected for the as-deposited films. However, the Ni(111) diffraction peak is observed for the $Zn_{0.83}Al_{0.06}Ni_{0.11}O$ and $Zn_{0.81}Al_{0.04}Ni_{0.15}O$ films magnetically annealed. The mean crystallite size D of Ni can be given by Scherrer's equation

$$D = \frac{0.89\lambda}{\beta\cos\theta} \quad (2)$$

where λ is the X-ray wavelength (0.15417 nm) and β the half-height width of the X-ray diffraction peak. θ is the Bragg angle. Using Eq. (2), according to the β value of the Ni(111) peak, the mean crystallite size of Ni is calculated to be about 20 nm. It is considered that the Ni nano-clusters exist in the Ni and Al co-doped ZnO films as-deposited and annealed although they can't be detected by XRD for the as-deposited films. We do not exclude the possibility forming the Ni nano-clusters small enough not to be detected by XRD. The Ni nano-clusters could exist at the grain boundaries in the polycrystalline films consisting of fine grains. After the films were magnetically annealed, the Ni nano-clusters grew and could be detected by XRD. In fact, X-ray photoelectron spectroscopy has also revealed that the metallic Ni existed in the Ni and Al co-doped ZnO films [19].

According to the XRD measurements, spacings of the (100), (002), (101) and (110) planes in the Ni and Al co-doped ZnO films can be obtained. Then the lattice volume of the films as-deposited and annealed are calculated and summarized in Table 2. As shown in Table 2, for the as-deposited $Zn_{0.87}Al_{0.06}Ni_{0.07}O$ film, the lattice volume is smaller than that of the ZnO bulk (47.62×10^{-3} nm) [18]. Ionic radii of Al^{3+} (0.57 Å) and Ni^{2+} (0.69 Å) are smaller than ionic radius of Zn^{2+} (0.74 Å). Therefore, the substitution of the Al^{3+} and/or Ni^{2+} ions for the Zn^{2+} ions results in the decrease in the lattice volume of the as-deposited $Zn_{0.87}Al_{0.06}Ni_{0.07}O$ film. For the $Zn_{0.83}Al_{0.06}Ni_{0.11}O$ and $Zn_{0.81}Al_{0.04}Ni_{0.15}O$ films, their lattice volumes are larger than that of the ZnO bulk. Furthermore, the lattice volume increases with increasing the Ni content. It suggests that some Ni and/or Al atoms enter into the interstitial sites of the ZnO lattice. The lattice volumes of the annealed films shrink compared with the as-deposited films and are smaller than that of the ZnO bulk. It means that the interstitial Ni atoms aggregate forming the Ni clusters during the magnetic annealing process. The Ni clusters could exist at the grain boundaries for the polycrystalline films. It should be noted that the Ni(111) diffraction peak from the Ni nano-clusters has been observed for the $Zn_{0.83}Al_{0.06}Ni_{0.11}O$ and $Zn_{0.81}Al_{0.04}Ni_{0.15}O$ films magnetically annealed.

Fig. 2 shows FE-SEM microphotographs of the Ni and Al co-doped ZnO films as-deposited and magnetically annealed. As can be seen from Fig. 2, all the films grow with thin columnar grains perpendicular to the substrate. Fig. 3 show AFM images of the Ni and Al co-doped ZnO films as-deposited and magnetically annealed. As shown in Fig. 3, the grain size of the films slightly decreases with increasing the Ni content. It is attributed to the impurity effect of Ni on the film structure. Namely, the more Ni atoms as impurity can lead to a high nucleation density at the initial stage of the film growth, decreasing the grain size of the film. The magnetic annealing promotes a slight growth of the grain size. Root mean square (RMS) roughnesses of the $Zn_{0.87}Al_{0.06}Ni_{0.07}O$, $Zn_{0.83}Al_{0.06}Ni_{0.11}O$ and $Zn_{0.81}Al_{0.04}Ni_{0.15}O$ films as-deposited are 4.6 ± 0.1 nm, 4.3 ± 0.1 nm and 5.0 ± 0.1 nm, respectively. After magnetically annealed, the RMS roughness of the $Zn_{0.83}Al_{0.06}Ni_{0.11}O$ film doesn't change markedly whereas the roughness of the $Zn_{0.87}Al_{0.06}Ni_{0.07}O$ film decreases to 2.48 ± 0.07 nm and that of the $Zn_{0.81}Al_{0.04}Ni_{0.15}O$ film increases to 6.0 ± 0.2 nm.

Table 2
Lattice volumes of the as-deposited and annealed films.

Film	Treatment	Lattice volume ($\times10^{-3}$ nm^3)
$Zn_{0.87}Al_{0.06}Ni_{0.07}O$	As-deposited	47.53
$Zn_{0.83}Al_{0.06}Ni_{0.11}O$	As-deposited	47.82
$Zn_{0.81}Al_{0.04}Ni_{0.15}O$	As-deposited	48.12
$Zn_{0.87}Al_{0.06}Ni_{0.07}O$	Annealed	47.41
$Zn_{0.83}Al_{0.06}Ni_{0.11}O$	Annealed	46.96
$Zn_{0.81}Al_{0.04}Ni_{0.15}O$	Annealed	47.22

3.2. Magnetic properties

Fig. 4 shows magnetization curves of the Ni and Al co-doped ZnO films as-deposited and magnetically annealed. For the films as-deposited, the $Zn_{0.87}Al_{0.06}Ni_{0.07}O$ film doesn't show any magnetic behavior whereas the $Zn_{0.83}Al_{0.06}Ni_{0.11}O$ and $Zn_{0.81}Al_{0.04}Ni_{0.15}O$ films exhibit magnetic hysteresis loops at room temperature, meaning that they have the room temperature ferromagnetism. After magnetically annealed, the $Zn_{0.87}Al_{0.06}Ni_{0.07}O$ film also has the room temperature ferromagnetism as shown in Fig. 4. Furthermore, the magnetic annealing markedly increases the saturation magnetization and the coercive force of the films. As a comparison, the Ni and Al co-doped films were annealed in vacuum at 673 K without magnetic field and their magnetization curves were measured by VSM. Fig. 5 shows the magnetization curves of the Ni and Al co-doped ZnO films annealed without magnetic field. Comparing Fig. 4 with Fig. 5, it can be concluded that the magnetic annealing more effectively enhances the saturation magnetization of the Ni and Al co-doped ZnO films relative to the annealing without magnetic field. In the present work, according to the XRD results, it is believed that the room temperature ferromagnetism of the films is attributed to the Ni nano-clusters forming in the films. It has been reported that for the Co doped ZnO films the room temperature ferromagnetism originates from the nano-sized Co clusters [20]. It has also been suggested that the ferromagnetism in the Co doped ZnO bulk is probably due to small clusters of second phase segregation [21]. For the as-deposited $Zn_{0.87}Al_{0.06}Ni_{0.07}O$ film, the Ni nano-clusters are too small to exhibit the room temperature ferromagnetism due to a low Curie temperature. The Curie temperature of the Ni nanocrystals decreased with decreasing the nanocrystal size and decreased dramatically when the nanocrystal size decreased below 10 nm [22]. For the Ni and Al co-doped ZnO films, the high Ni content and the magnetic annealing increase the size of the Ni nano-clusters. As a result, the $Zn_{0.83}Al_{0.06}Ni_{0.11}O$ and $Zn_{0.81}Al_{0.04}Ni_{0.15}O$ films as well as all the films annealed exhibit the room temperature ferromagnetism. The high saturation magnetization, residual magnetization and coercivity of the $Zn_{0.81}Al_{0.04}Ni_{0.15}O$ film magnetically annealed are attributed to a good crystallinity of the Ni nano-clusters.

Fig. 6 shows a temperature dependence of the magnetization (M–T curve) for the Ni and Al co-doped ZnO films magnetically annealed. As can be seen from Fig. 6, the Curie temperature is above 400 K for the annealed films. Furthermore, the annealed $Zn_{0.81}Al_{0.04}Ni_{0.15}O$ film has the least variation of magnetization with temperature. It has been reported that nanostructured Ni films with a porous thin columnar grains exhibited a faster decrease in the saturation magnetization with temperature and a lower Curie temperature compared with the films having a good crystallinity [23]. Therefore, it is considered that the Ni nano-clusters in the $Zn_{0.81}Al_{0.04}Ni_{0.15}O$ film magnetically annealed have a good crystallinity, resulting in the least variation of magnetization with temperature.

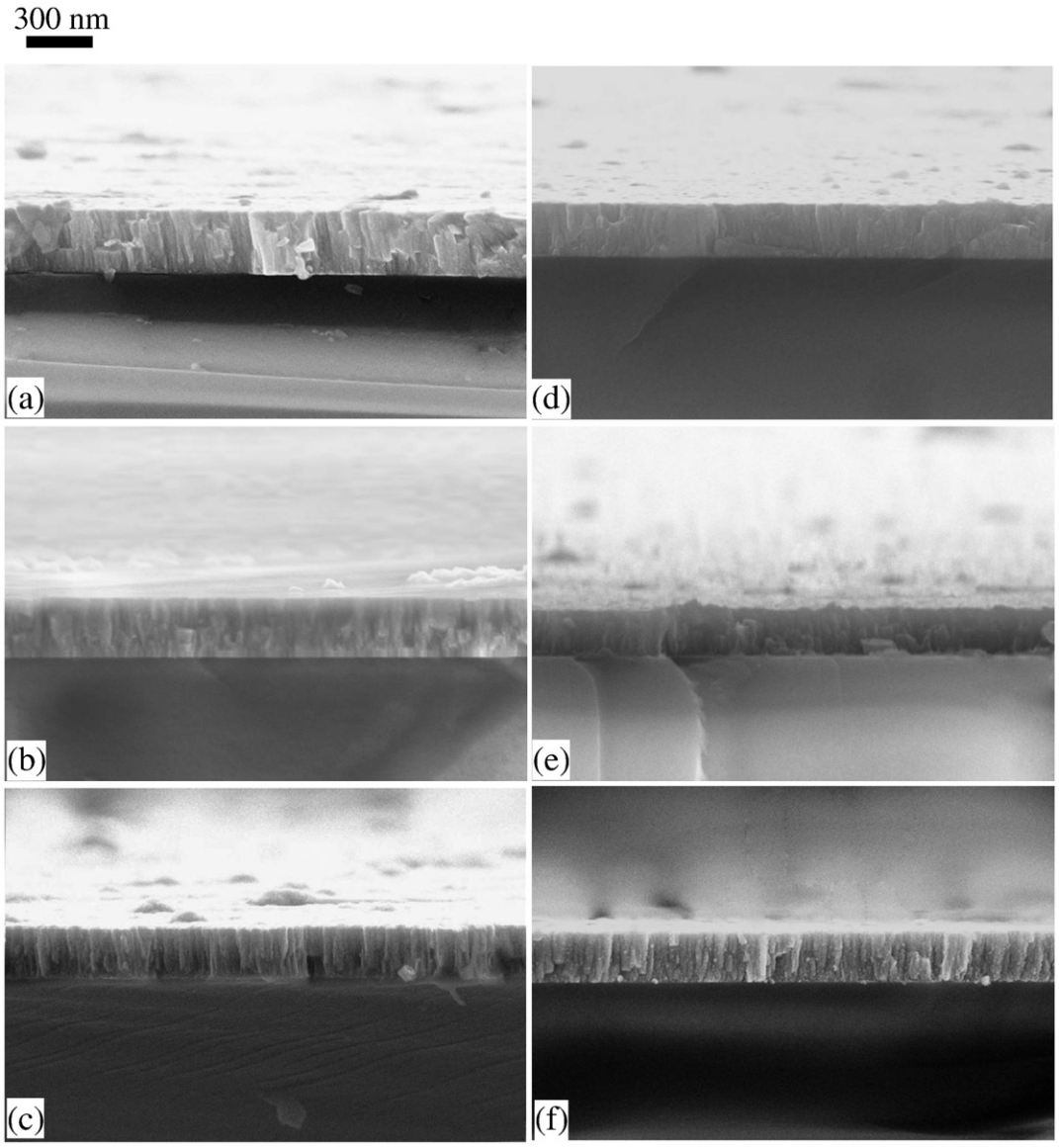

Fig. 2. FE-SEM microphotographs of the Ni and Al co-doped ZnO films; (a) $Zn_{0.87}Al_{0.06}Ni_{0.07}O$ film, as-deposited, (b) $Zn_{0.83}Al_{0.06}Ni_{0.11}O$ film, as-deposited, (c) $Zn_{0.81}Al_{0.04}Ni_{0.15}O$ film, as-deposited, (d) $Zn_{0.87}Al_{0.06}Ni_{0.07}O$ film, annealed, (e) $Zn_{0.83}Al_{0.06}Ni_{0.11}O$ film, annealed, (f) $Zn_{0.81}Al_{0.04}Ni_{0.15}O$ film, annealed.

Fig. 7 shows the magnetization curves of the Ni and Al co-doped films magnetically annealed, in which the magnetic field is applied parallel and perpendicular to the direction of the annealing magnetic field during the VSM measurements, respectively. As shown in Fig. 7, all the films exhibit an anisotropic magnetization behavior. The saturation magnetization and residual magnetization of the film at a measurement field parallel to the annealing field are larger than those of the film at a measurement field perpendicular to the annealing field. It indicates that some magnetic moments align along the direction of the annealing magnetic field. When the measurement field is applied along the direction of the annealing field, all the magnetic moments rotate easily to the direction of the measurement field. However, when the measurement field is applied perpendicular to the direction of the annealing field, some magnetic moments such as those along the annealing magnetic field could not rotate to the direction of the measurement field. Therefore, the films exhibit the anisotropic magnetization behavior. It should be noted that the alignment of magnetic moments is retained to some extent along the direction of the annealing field although the films are cooled down to room temperature from 673 K without magnetic field.

3.3. Electrical properties

All the Ni and Al co-doped films are an n-type semiconductor. The free electron concentrations, the Hall mobilities and the resistivities are summarized in Table 3. As shown in Table 3, for the as-deposited films, the $Zn_{0.87}Al_{0.06}Ni_{0.07}O$ film has the highest free electron concentration. The Hall mobility of the as-deposited films decreases markedly with increasing the Ni content. The resistivity is proportional to the reciprocal of the product of carrier concentration and Hall mobility. Therefore, the resistivity of the as-deposited films increases with increasing the Ni content. The annealing improves mainly the Hall mobility of the films. Furthermore, the annealing leads to a remarkable increase in the free electron concentration for the $Zn_{0.83}Al_{0.06}Ni_{0.11}O$ film. Finally, the annealing decreases the resistivity of the Ni and Al co-doped films. The $Zn_{0.87}Al_{0.06}Ni_{0.07}O$ film magnetically annealed has the lowest resistivity ($8.73\times10^{-3}\,\Omega$cm).

For the ZnO:Al films, Al atoms as donors are substitutively incorporated at the Zn sites in the ZnO lattice. Generally, it is considered that Ni^{2+} ions substitute for the Zn^{2+} ions in the Ni-doped ZnO film because Ni^{2+} ions are prone to be formed in the oxygen environment [12,24]. Therefore, the doping of Ni doesn't contribute to the increase in

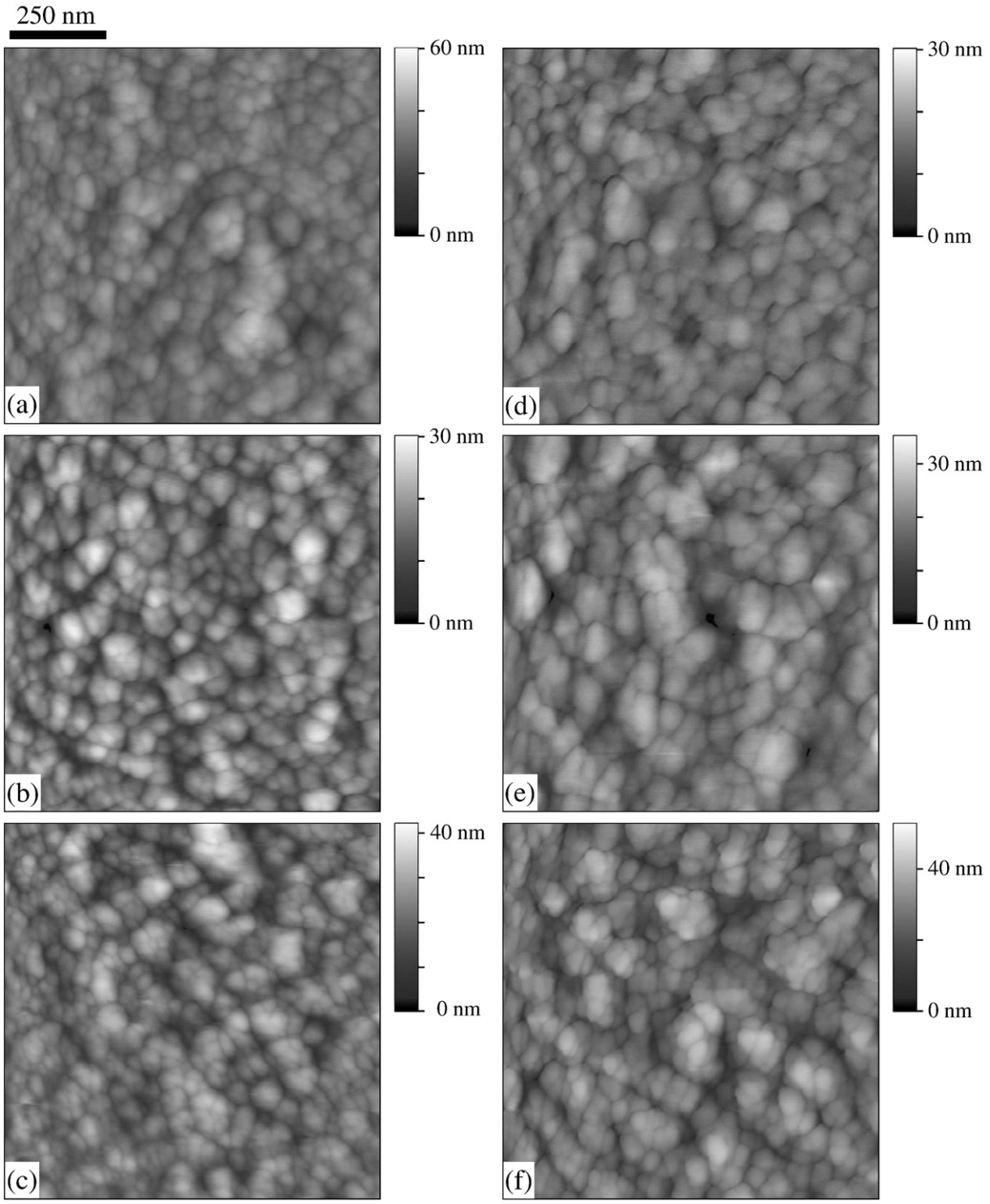

Fig. 3. AFM images of the Ni and Al co-doped ZnO films; (a) $Zn_{0.87}Al_{0.06}Ni_{0.07}O$ film, as-deposited, (b) $Zn_{0.83}Al_{0.06}Ni_{0.11}O$ film, as-deposited, (c) $Zn_{0.81}Al_{0.04}Ni_{0.15}O$ film, as-deposited, (d) $Zn_{0.87}Al_{0.06}Ni_{0.07}O$ film, annealed, (e) $Zn_{0.83}Al_{0.06}Ni_{0.11}O$ film, annealed, (f) $Zn_{0.81}Al_{0.04}Ni_{0.15}O$ film, annealed.

the carrier concentration for the Ni-doped ZnO films. For the Ni and Al co-doped ZnO films, under the assumption that every substitutive Al atom provides one free electron, the Al doping efficiency η is given by

$$\eta = \frac{n}{N}$$

$$N = \frac{n_0 \times N_0}{\frac{\sqrt{3}}{2} \times a^2 \times c} \tag{3}$$

where n is the free electron concentration measured. N is the Al actual concentration in the film when all the Al^{3+} ions substitute for the Zn^{2+} ions in the ZnO lattice. n_0 is the number of Zn atoms in an unit cell and is equal to 2. a and c, which are determined by the XRD measurements, are the lattice constants along a-axis and c-axis. N_0 is the Al actual atomic content. According to Eq. (3), the Al doping efficiency is calculated. The maximal Al doping efficiency is obtained to be about 7% for the $Zn_{0.87}Al_{0.06}Ni_{0.07}O$ film magnetically annealed. In the present work, the Al doping efficiency is very low. The Al

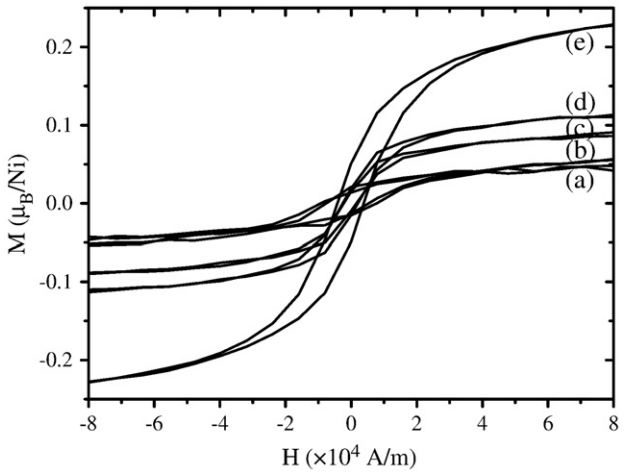

Fig. 4. Magnetizition curves of the Ni and Al co-doped ZnO films; (a) $Zn_{0.83}Al_{0.06}Ni_{0.11}O$ film, as-deposited, (b) $Zn_{0.81}Al_{0.04}Ni_{0.15}O$ film, as-deposited, (c) $Zn_{0.87}Al_{0.06}Ni_{0.07}O$ film, annealed, (d) $Zn_{0.83}Al_{0.06}Ni_{0.11}O$ film, annealed, (e) $Zn_{0.81}Al_{0.04}Ni_{0.15}O$ film, annealed.

doping efficiency can be controlled by the competition of the substitution of Ni^{2+} and Al^{3+} ions for the Zn^{2+} ions. As the Ni content in the films increases, many Ni^{2+} ions occupy the Zn^{2+} sites, leading to a decrease in the Al^{3+} ions substituting for the Zn^{2+} ions. Therefore, the high Ni content lowers the Al doping efficiency and the free electron concentration in the Ni and Al co-doped ZnO films. Furthermore, the films grow with thin columnar grains. The Al atoms not substituting for Zn^{2+} ions in the ZnO lattice can exist at the grain boundaries and don't play the donor role. On the other hand, for the films having the high Ni content, some Ni atoms could enter into the interstitial sites of the ZnO lattice as indicated by the XRD results and promote a formation of the defects with incomplete atomic bonds. The Ni interstitial atoms and the defects could form the scattering centers of free electrons. Therefore, for the as-deposited films the Hall mobility decreases with increasing the Ni content. When the films were magnetically annealed, the crystallinity of the films is improved as indicated by the AFM results and the Ni interstitial atoms aggregate promoting the growth of the Ni nano-clusters as indicated by the XRD results. The Ni nano-clusters could exist at the grain boundaries. It is considered that the annealing decreases the defects and the Ni interstitial atoms in the films, decreasing the scattering centers of free electrons. As a result, the annealing enhances the Hall mobility in the Ni and Al co-doped ZnO films.

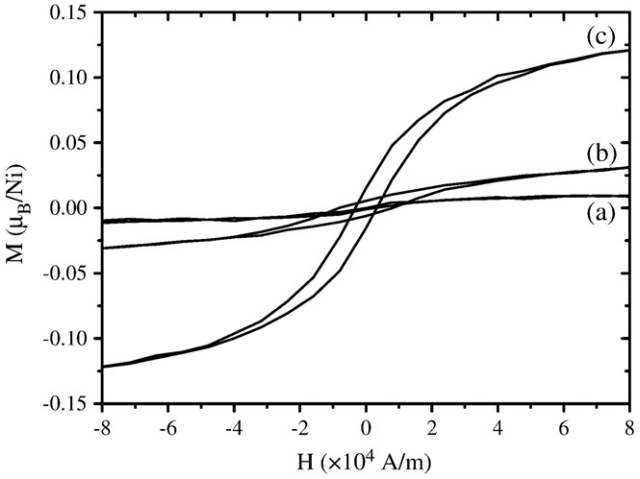

Fig. 5. Magnetizition curves of the Ni and Al co-doped ZnO films annealed without magnetic field; (a) $Zn_{0.87}Al_{0.06}Ni_{0.07}O$ film, (b) $Zn_{0.83}Al_{0.06}Ni_{0.11}O$ film, (c) $Zn_{0.81}Al_{0.04}Ni_{0.15}O$ film.

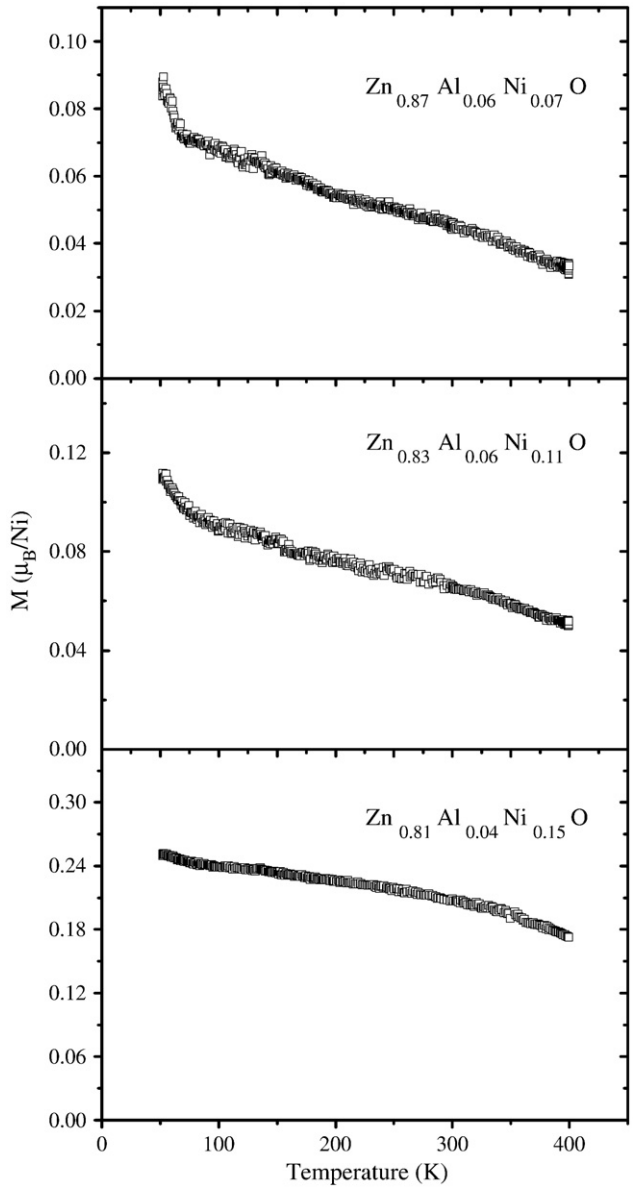

Fig. 6. M–T curves of the Ni and Al co-doped ZnO films magnetically annealed.

Fig. 8 show a temperature dependence of the resistance for the Ni and Al co-doped ZnO films as-deposited and magnetically annealed. In Fig. 8, the resistance R_T at each temperature is normalized to the resistance R_{300K} at 300 K. As can be seen from Fig. 8, the resistivity of the films decreases with increasing temperature. It exhibits a semiconducting behavior. For the Al-doped ZnO films, the Zn interstitial atoms, the O vacancies and the Al substitutive atoms in the Zn lattice sites contribute to donors [25]. Generally, it is considered that Ni^{2+} ions substitute for the Zn^{2+} ions in the Ni-doped ZnO film [12,24] and the doping of Ni doesn't contribute to the increase in the carrier concentration for the Ni-doped ZnO films.

The scattering mechanism of the carrier might mainly include ionized impurity scattering, grain boundary scattering and lattice vibration scattering. The mean free path L of electrons in the films can be given by [26]

$$L = \left(\frac{h}{2e}\right)\left(\frac{3n}{\pi}\right)^{\frac{1}{3}}\mu \tag{4}$$

where n is the free electron concentration and μ is the Hall mobility. h is the Planck constant and e is the elementary charge. Using the n

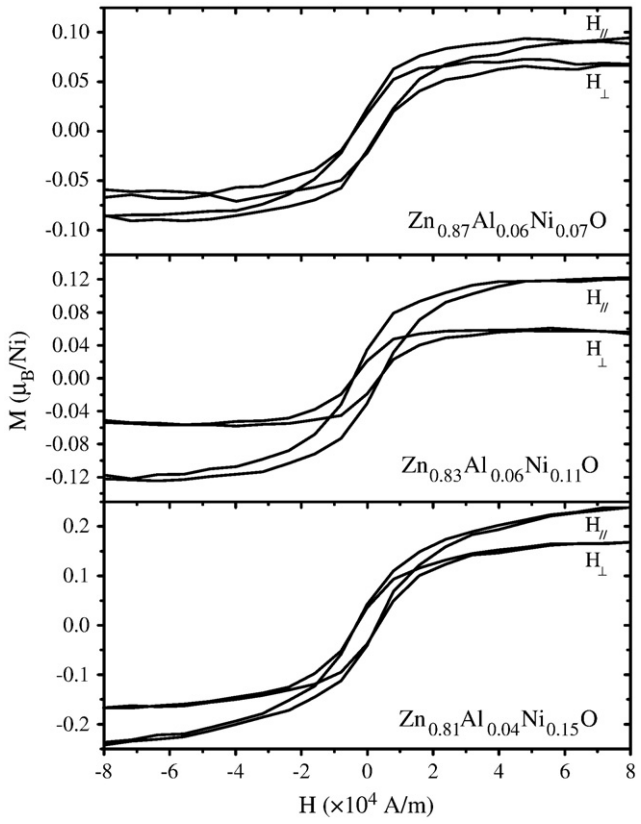

Fig. 7. Magnetization curves of the Ni and Al co-doped ZnO films magnetically annealed. The magnetic field is applied parallel and perpendicular to the direction of the annealing magnetic field during the VSM measurements.

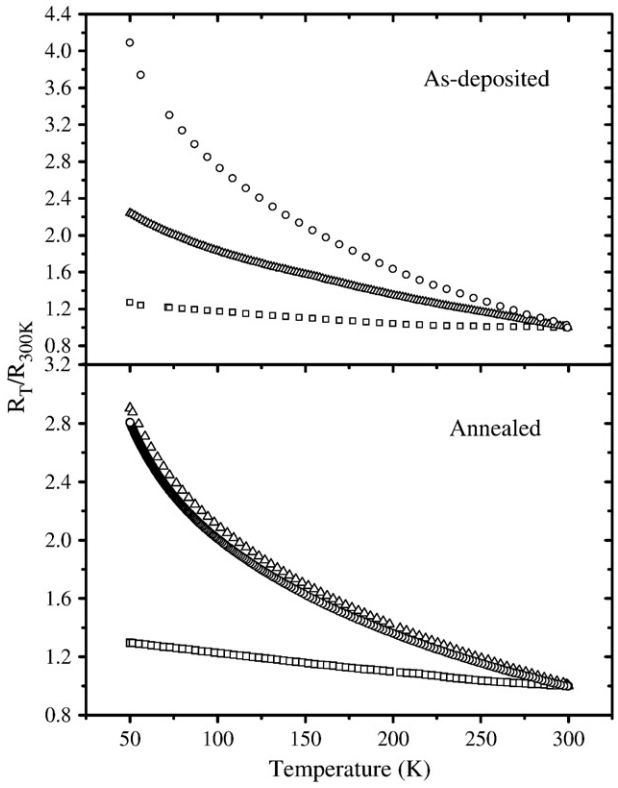

Fig. 8. Temperature dependence of the resistance for the Ni and Al co-doped ZnO films as-deposited and magnetically annealed. □: $Zn_{0.87}Al_{0.06}Ni_{0.07}O$ film, △: $Zn_{0.83}Al_{0.06}Ni_{0.11}O$ film, ○: $Zn_{0.81}Al_{0.04}Ni_{0.15}O$ film.

and μ values obtained, the mean free path of the electrons is estimated to be significantly small relative to the grain size of the films. Therefore, in this case the grain boundary scattering might be negligible. The carrier mobility μ_I due to the ionized impurity scattering for a non-degenerate semiconductor is given by

$$\mu_I \propto T^{\frac{3}{2}} \tag{5}$$

and that μ_P due to the lattice vibration scattering is expressed as

$$\mu_P \propto T^{-\frac{3}{2}} \tag{6}$$

where T is the absolute temperature [27,28]. For the thermally activated band conduction, the free electron concentration n can be given by [29]

$$n = N_C \exp\left(-\frac{\Delta E_A}{kT}\right) \tag{7}$$

where N_C is a constant related to the material and ΔE_A is the activation energy. k is the Boltzmann constant.

Table 3
Electron concentrations n, Hall mobilities μ and resistivities ρ of the as-deposited and annealed films.

Film	Treatment	n (cm^{-3})	μ (cm^2/V s)	ρ (Ω cm)
$Zn_{0.87}Al_{0.06}Ni_{0.07}O$	As-deposited	1.50×10^{20}	2.70	1.54×10^{-2}
$Zn_{0.83}Al_{0.06}Ni_{0.11}O$	As-deposited	2.4×10^{18}	0.20	15.5
$Zn_{0.81}Al_{0.04}Ni_{0.15}O$	As-deposited	4.26×10^{18}	0.06	18.9
$Zn_{0.87}Al_{0.06}Ni_{0.07}O$	Annealed	1.73×10^{20}	4.16	8.73×10^{-3}
$Zn_{0.83}Al_{0.06}Ni_{0.11}O$	Annealed	1.27×10^{20}	3.18	1.6×10^{-2}
$Zn_{0.81}Al_{0.04}Ni_{0.15}O$	Annealed	2.35×10^{18}	1.20	2.23

The resistivity is proportional to the reciprocal of the product of carrier concentration and Hall mobility. First, it is considered that the free electron mobility is dominated by the ionized impurity scattering. Using Eqs. (5) and (7), the resistivity ρ of the film is expressed as

$$\rho \propto T^{-\frac{3}{2}} \exp\left(\frac{\Delta E_A}{kT}\right). \tag{8}$$

On the other hand, it was reported that the conduction mechanism due to the thermal activation occurred at temperatures over 200 K for the ZnO: Al films [30] and the ZnO films [28,31]. According to Eq. (8), a variation of $\ln(\rho T^{3/2})$ with T^{-1} is plotted in Fig. 9. As can be seen from Fig. 9, for all the films, the plot over 200 K exhibits a well linear dependence. However, a negative activation energy is obtained in terms of the slope of the straight line. It indicates that the ionized impurity scattering could not dominate the free electron transport in the films. Then, using Eqs. (6) and (7), the resistivity ρ of the film is given by

$$\rho \propto T^{\frac{3}{2}} \exp\left(\frac{\Delta E_A}{kT}\right). \tag{9}$$

Fig. 10a shows a temperature dependence of the resistivity for the Ni and Al co-doped ZnO films as-deposited and magnetically annealed, plotted as $\ln(\rho T^{-3/2})$ versus T^{-1}. As can be seen from Fig. 10a, the plot can't exhibit the linear relationship in the whole measuring temperature range of 50–300 K, meaning that the free electron transport is not dominated by the single scattering mechanism. It is generally considered that the lattice vibration scattering is predominant at the relatively high temperature. As shown in Fig. 10b, a good linear dependence having a linearity factor better than 0.995 is exhibited in the high temperature region. The activation energy is calculated in terms of the slope of the fitted straight line. The activation

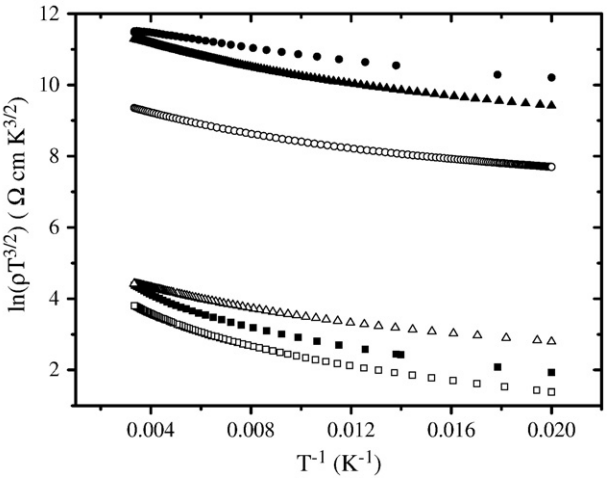

Fig. 9. Variation of $\ln(\rho T^{3/2})$ with T^{-1} for the Ni and Al co-doped ZnO films. ■: $Zn_{0.87}Al_{0.06}Ni_{0.07}O$ film, as-deposited, ▲: $Zn_{0.83}Al_{0.06}Ni_{0.11}O$ film, as-deposited, ●: $Zn_{0.81}Al_{0.04}Ni_{0.15}O$ film, as-deposited, □: $Zn_{0.87}Al_{0.06}Ni_{0.07}O$ film, annealed, △: $Zn_{0.83}Al_{0.06}Ni_{0.11}O$ film, annealed, ○: $Zn_{0.81}Al_{0.04}Ni_{0.15}O$ film, annealed.

energies for $Zn_{0.87}Al_{0.06}Ni_{0.07}O$, $Zn_{0.83}Al_{0.06}Ni_{0.11}O$ and $Zn_{0.81}Al_{0.04}Ni_{0.15}O$ films as-deposited are 36 meV, 56 meV and 65 meV while those magnetically annealed are 35 meV, 54 meV and 54 meV, respectively. Considering the change in the free electron concentration, it can be said that the activation energy for the thermally activated band conduction depends on the carrier concentration and the impurity energy level. An increase in the carrier concentration raises the Fermi energy to a high level in the energy gap, leading to the decrease in the activation energy [32]. For the low temperature region, the plot shown in Fig. 10a also exhibits a good linear dependence. The fitted activation energies are lower than 9 meV and are very small. It means that a different carrier transport mechanism, i.e., not thermally activated band conduction, dominates at the low temperatures for the Ni and Al co-doped ZnO films.

At low temperatures the carrier transport mechanism can be explained using the variable range hopping (VRH) model proposed by Mott. The electrons hop between the localized states. These localized states exist inside the energy distribution region of the impurity level in the energy gap. The electron hops from the occupied localized state to the unoccupied one under the favourable condition. In the Mott's VRH model, a relationship between the conductivity σ and the temperature T is given by [28,30–32]

$$\sigma = \sigma_0 T^{-\frac{1}{2}} \exp\left[-\left(\frac{T_0}{T}\right)^{\frac{1}{4}}\right] \tag{10}$$

where σ_0 and T_0 are expressed as

$$\sigma_0 = \frac{3e^2\nu_P}{\sqrt{8\pi}} \times \left[\frac{N(E_F)}{\alpha kT}\right]^{\frac{1}{2}} \tag{11}$$

$$T_0 = \frac{16\alpha^3}{kN(E_F)} \tag{12}$$

where ν_P is the phonon frequency ($\approx 10^{13}$ Hz) at Debye temperature. $N(E_F)$ is the density of the localized electron states at Fermi level. α is the inverse localization length of wave function associated with the localized state. Fig. 11 shows a temperature dependence of the conductivity for the Ni and Al co-doped ZnO films as-deposited and magnetically annealed, plotted as $\ln(\sigma T^{1/2})$ versus $T^{-1/4}$. As can be seen from Fig. 11, the plot can't exhibit the linear relationship in the whole measuring temperature range of 50–300 K. However, it exhibits a good linear dependence having a linearity factor of 0.998 in the low temperature range. According to Eq. (10), the T_0 value is calculated in terms of the slope of the fitted straight line and the σ_0 value is obtained by the intercept of the fitted line and the $\ln(\sigma T^{1/2})$ axis. The T_0 and σ_0 values are summarized in Table 4. Using Eqs. (11) and (12), $N(E_F)$ and α are calculated and also listed in Table 4. As shown in Table 4, the as-deposited $Zn_{0.87}Al_{0.06}Ni_{0.07}O$ film as well as the $Zn_{0.87}Al_{0.06}Ni_{0.07}O$ and $Zn_{0.83}Al_{0.06}Ni_{0.11}O$ films magnetically annealed have the high density of the localized electron state and the narrow localization length of the wave function. For the Ni and Al co-doped ZnO films, the high crystallinity results in the high density of the localized state and the narrow localization length of the wave

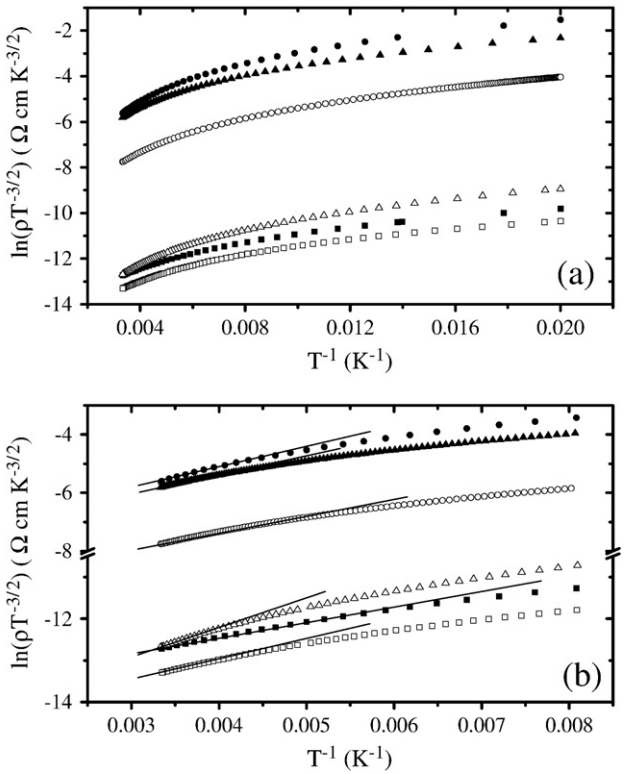

Fig. 10. Variation of $\ln(\rho T^{-3/2})$ with T^{-1} for the Ni and Al co-doped ZnO films. ■: $Zn_{0.87}Al_{0.06}Ni_{0.07}O$ film, as-deposited, ▲: $Zn_{0.83}Al_{0.06}Ni_{0.11}O$ film, as-deposited, ●: $Zn_{0.81}Al_{0.04}Ni_{0.15}O$ film, as-deposited, □: $Zn_{0.87}Al_{0.06}Ni_{0.07}O$ film, annealed, △: $Zn_{0.83}Al_{0.06}Ni_{0.11}O$ film, annealed, ○: $Zn_{0.81}Al_{0.04}Ni_{0.15}O$ film, annealed.

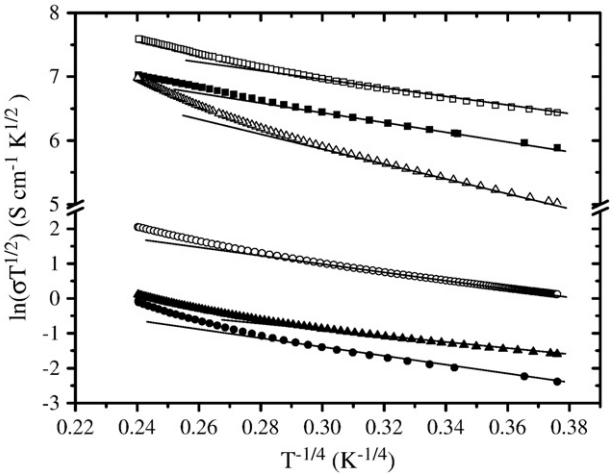

Fig. 11. Variation of $\ln(\sigma T^{1/2})$ with $T^{-1/4}$ for the Ni and Al co-doped ZnO films. ■: $Zn_{0.87}Al_{0.06}Ni_{0.07}O$ film, as-deposited, ▲: $Zn_{0.83}Al_{0.06}Ni_{0.11}O$ film, as-deposited, ●: $Zn_{0.81}Al_{0.04}Ni_{0.15}O$ film, as-deposited, □: $Zn_{0.87}Al_{0.06}Ni_{0.07}O$ film, annealed, △: $Zn_{0.83}Al_{0.06}Ni_{0.11}O$ film, annealed, ○: $Zn_{0.81}Al_{0.04}Ni_{0.15}O$ film, annealed.

Table 4
σ_0 data, T_0 data, inverse localization lengths α and the densities of localized states $N(E_F)$ of the as-deposited and annealed films.

Film	Treatment	σ_0 (S cm^{-1} K$^{1/2}$)	T_0 (K)	α (cm^{-1})	$N(E_F)$
$Zn_{0.87}Al_{0.06}Ni_{0.07}O$	As-deposited	6365.2	3512.8	8.5×10^{6}	3.2×10^{22}
$Zn_{0.83}Al_{0.06}Ni_{0.11}O$	As-deposited	6.0	6565.3	1.1×10^{4}	3.6×10^{13}
$Zn_{0.81}Al_{0.04}Ni_{0.15}O$	As-deposited	9.7	23388.4	3.3×10^{4}	2.9×10^{14}
$Zn_{0.87}Al_{0.06}Ni_{0.07}O$	Annealed	7676.8	2000.7	7.7×10^{6}	4.3×10^{22}
$Zn_{0.83}Al_{0.06}Ni_{0.11}O$	Annealed	11140.3	17211.9	3.3×10^{7}	3.9×10^{23}
$Zn_{0.81}Al_{0.04}Ni_{0.15}O$	Annealed	84.1	17314.3	2.5×10^{5}	1.7×10^{17}

function. This result is consistent with that reported previously for the ZnO:Al films [33]. Finally, the carrier transport mechanism in the Ni and Al co-doped ZnO film is the Mott's variable range hopping in the low temperature range and the thermally activated band conduction in the high temperature range.

5. Summary

The $Zn_{0.87}Al_{0.06}Ni_{0.07}O$, $Zn_{0.83}Al_{0.06}Ni_{0.11}O$ and $Zn_{0.81}Al_{0.04}Ni_{0.15}O$ films were sputter-deposited on glass substrates at 300 K and then were annealed in vacuum at 673 K under the magnetic field. All the films have a wurtzite structure and consist of thin columnar grains perpendicular to the substrate. The annealing promotes the (002) orientation growth in the film growing direction for the $Zn_{0.87}Al_{0.06}Ni_{0.07}O$ and $Zn_{0.83}Al_{0.06}Ni_{0.11}O$ films as well as the (100) orientation growth for the $Zn_{0.81}Al_{0.04}Ni_{0.15}O$ film. The annealing results in the slight increase in the grain size. A weak Ni diffraction peak was detected for the annealed films with high Ni content. The annealing enhances the room temperature ferromagnetism of the films. The Curie temperature is above 400 K for the annealed films. The films magnetically annealed exhibit the anisotropic magnetization behavior. The annealed $Zn_{0.87}Al_{0.06}Ni_{0.07}O$ film has the lowest resistivity ($8.73\times10^{-3}\,\Omega$cm), the highest free electron concentration (1.73×10^{20} cm^{-3}) and Hall mobility (4.16 cm^{2}V^{-1} s^{-1}). The carrier transport mechanism is Mott's variable range hopping in the low temperature range and thermally activated band conduction in the high temperature range.

Acknowledgements

The authors would like to thank Ms. J. P. He of the State Key Laboratory for Advanced Metals and Materials for FE-SEM observations. The financial support from the Scientific Research Fund of Beijing Municipal Commission of Education Project 2009 is gratefully acknowledged.

References

[1] M. Venkatesan, P. Stamenov, L.S. Dorneles, R.D. Gunning, B. Bernoux, J.M.D. Coey, Appl. Phys. Lett. 90 (2007) 242508.
[2] A.J. Behan, A. Mokhtari, H.J. Blythe, D. Score, X.H. Xu, J.R. Neal, A.M. Fox, D.A. Gehring, Phys. Rev. Lett. 100 (2008) 047206.
[3] K. Samanta, P. Bhattacharya, J.G.S. Duque, W. Iwamoto, C. Rettori, P.G. Pagliuso, R.S. Katiyar, Solid State Commun. 147 (2008) 305.
[4] M. Sharma, R.M. Mehra, Appl. Surf. Sci. 255 (2008) 2527.
[5] S.K. Neogi, R. Ghosh, G.K. Paul, S.K. Bera, S. Bandyopadhyay, J. Alloys Compd. 487 (2009) 269.
[6] T.F. Li, H. Qiu, P. Wu, M.W. Wang, R.X. Ma, Thin Solid Films 515 (2007) 3905.
[7] M.P. Yu, H. Qiu, X.B. Chen, H.X. Liu, M.W. Wang, Physica B 404 (2009) 1829.
[8] Y.M. Cho, W.K. Choo, H. Kim, D. Kim, Y. Ihm, Appl. Phys. Lett. 80 (2002) 3358.
[9] H.S. Hsu, J.C.A. Huang, Y.H. Huang, Y.F. Liao, M.Z. Lin, C.H. Lee, J.F. Lee, S.F. Chen, L.Y. Lai, C.P. Liu, Appl. Phys. Lett. 88 (2006) 242507.
[10] N. Khare, M.J. Kappers, M. Wei, M.G. Blamire, J.L. MacManus-Driscoll, Adv. Mater. 18 (2006) 1449.
[11] B. Huang, D.L. Zhu, X.C. Ma, Appl. Surf. Sci. 253 (2007) 6892.
[12] E. Liu, P. Xiao, J.S. Chen, B.C. Lim, L. Lia, Curr. Appl Phys. 8 (2008) 408.
[13] K. Harada, S. Tsurekawa, T. Watanabe, G. Palumbo, Scr. Mater. 49 (2003) 367.
[14] J.K. Chung, W.J. Kim, S.G. Lee, C.J. Kim, J. Alloys Compd. 449 (2008) 180.
[15] M. Coisson, F. Celegato, P. Tiberto, F. Vinai, J. Magn. Magn. Mater. 320 (2008) e739.
[16] X.B. Chen, H. Qiu, H. Qian, P. Wu, F.P. Wang, L.Q. Pan, Y. Tian, Vacuum 75 (2004) 217.
[17] K. Sumi, H. Qiu, K. Kamei, S. Moriya, M. Murai, M. Shimada, T. Nishiwaki, K. Tahei, M. Hashimoto, Thin Solid Films 349 (1999) 270.
[18] Powder Diffraction File, Joint Committee on Powder Diffraction Standards, Bethlehem, PA, JCPDS Card 36-1451, 1986.
[19] M.P. Yu, H. Qiu, X.B. Chen, H.X. Liu, Mater. Chem. Phys. 120 (2010) 571.
[20] J.H. Park, M.G. Kim, H.M. Jang, S. Ryu, M.Y. Kim, Appl. Phys. Lett. 84 (2004) 1338.
[21] S. Yin, M.X. Xu, L. Yang, J.F. Liu, H. Roner, H. Hahn, H. Gleiter, D. Schild, S. Doyle, T. Liu, T.D. Hu, E.T. Muromachi, J.Z. Jiang, Phys. Rev. B 73 (2006) 224408.
[22] H.M. Lu, P.Y. Li, Y.N. Huang, X.K. Meng, X.Y. Zhang, Q. Liu, J. Appl. Phys. 105 (2009) 023516.
[23] H. Qiu, M.P. Yu, J. Shi, Y. Nakamura, S. Nagayama, M. Hashimoto, Vacuum 82 (2008) 1318.
[24] Z. Yin, N. Chen, F. Yang, S. Song, C. Chai, J. Zhong, H. Qian, K. Ibrahim, Solid State Commun. 135 (2005) 430.
[25] Y. Igasaki, H. Saito, J. Appl. Phys. 69 (1991) 2190.
[26] Y.G. Wang, S.P. Lau, H.W. Lee, S.F. Yu, B.K. Tay, X.H. Zhang, K.Y. Tse, H.H. Hng, J. Appl. Phys. 94 (2003) 1597.
[27] A. Boulouz, S. Chakraborty, A. Giani, F.P. Delannoy, A. Boyer, J. Schumann, J. Appl. Phys. 89 (2001) 5009.
[28] Y. Natsume, H. Sakata, Mater. Chem. Phys. 78 (2002) 170.
[29] A.E.J. Gonzalez, J.A.S. Urueta, R.S. Parra, J. Cryst. Growth 192 (1998) 430.
[30] S. Bandyopadhyay, G.K. Paul, R. Roy, S.K. Sen, S. Sen, Mater. Chem. Phys. 74 (2002) 83.
[31] N. Brilis, D. Tsamakis, H. Ali, S. Krishnamoorthy, A.A. Iliadis, Thin Solid Films 516 (2008) 4226.
[32] R. Kumar, N. Khare, Thin Solid Films 516 (2008) 1302.
[33] H.X. Liu, H. Qiu, X.B. Chen, M.P. Yu, M.W. Wang, Curr. Appl Phys. 9 (2009) 1217.